J Mol Model (2011) 17:533–541
DOI 10.1007/s00894-010-0744-2

ORIGINAL PAPER

Structural and docking studies of *Leucaena leucocephala* Cinnamoyl CoA reductase

Nirmal K. Prasad · Vaibhav Vindal · Vikash Kumar · Ashish Kabra · Navneet Phogat · Manoj Kumar

Received: 19 February 2010 / Accepted: 4 May 2010 / Published online: 29 May 2010

Abstract Lignin, a major constituent of plant call wall, is a phenolic heteropolymer. It plays a major role in the development of plants and their defense mechanism against pathogens. Therefore Lignin biosynthesis is one of the critical metabolic pathways. In lignin biosynthesis, the Cinnamoyl CoA reductase is a key enzyme which catalyzes the first step in the pathway. Cinnamoyl CoA reductase provides the substrates which represent the main transitional molecules of lignin biosynthesis pathway, exhibits a high *in vitro* kinetic preference for feruloyl CoA. In present study, the three-dimensional model of cinnamoyl CoA reductase was constructed based on the crystal structure of Grape Dihydroflavonol 4-Reductase. Furthermore, the docking studies were performed to understand the substrate interactions to the active site of CCR. It showed that residues ARG51, ASN52, ASP54 and ASN58 were involved in substrate binding. We also suggest that residue ARG51 in CCR is the determinant residue in competitive inhibition of other substrates. This structural and docking information have prospective implications to understand the mechanism of CCR enzymatic reaction with feruloyl CoA, however the approach will be applicable in prediction of substrates and engineering 3D structures of other enzymes as well.

N. K. Prasad (✉) · V. Kumar · A. Kabra · N. Phogat · M. Kumar
Department of Biotechnology, Goa University,
Taleigao Plateau,
Goa, India 403206
e-mail: nimmynirmal@gmail.com

V. Vindal
Department of Biotechnology and Bioinformatics Infrastructure Facility, University of Hyderabad,
Gachibowli,
Hyderabad 500046, India

Keywords Cinnamoyl CoA reductase · Docking · Feruloyl CoA · *Leucaena leucocephala* · Lignin biosynthesis

Introduction

Cinnamoyl CoA reductase (CCR), one of the key enzyme in lignin synthesis, catalyzes the NADPH dependent reduction of p-hydroxycinnamoyl CoA, the phenyl propanoid pathway metabolites, to p-hydroxycinnamaldehydes. These are further catalyzed by enzyme cinnamoyl alcohol dehydrogenase (CAD) to monolignols [1–6]. The later are involved in oxidative polymerization process, catalyzed by NADPH oxidase, resulting into the synthesis of cross linked plant polymer lignin. It plays an important role in plant defense responses which act as a mechanical barrier to various plant pathogens [7–10]. Reduction in lignin content is always desirable in pulp and paper industry as lignin is one of the obstacles for good quality product synthesis and makes the process costlier [5]. Being the first committed enzyme of monolignol biosynthesis and directing the metabolite flux of phenyl propanoid pathway towards lignin synthesis, CCR shows an association with lignin biosynthesis. It has been demonstrated that the down regulation of CCR in transgenic tobacco, arabidopsis and tomato, leads to the significant reduction of lignin content and distinct pH requirement for its catalysis as compared to the neighboring reactions catalyzed by other enzymes. These reasons indicate CCR as a strong control point for regulating lignin content [1–3, 7, 8]. On the basis of mutant analysis in *Arabidopsis thaliana*, it was examined that the alternative splicing in CCR region is responsible for affecting the physical properties of cell wall such as stiffness and strength [2, 11]. CCR is also believed to be involved in regulating stem rigidity in wheat, reported

Table 1 Target and template proteins information

Target	Template		
	PDB ID	Protein	Sequence identity
CCR	2C29	Dihydroflavonol-4-reductase, chain D	43%
	2RH8	Apo Anthocyanidin Reductase, chian A	37%
	2P4H	Vestitone Reductase	33%

according to the parallel correlation existing between *Triticum aestivum* CCR1 (TaCCR1) mRNA level and high CCR activity present in wheat stem [8]. CCR acts at optimum pH of 6.25 for its catalytic activities, as reported in *Arabidopsis thaliana*, *Eucalyptus gunii* (crude protein extract and purified one), poplar stems, spruce and soya bean extract [5, 12–15]. As already reported in case of wheat, TaCCR1 and TaCCR2 are known to exhibit differences in their primary amino acid sequences, but they have identical motifs for NADPH binding and active site [7]. CCR exhibits the substrate specificity with feruloyl CoA, caffeoyl CoA, 5-hydroxyferuloyl CoA and sinapoyl CoA, converting them into their respective products coniferaldehyde, caffealdehyde, 5-hydroxyconiferaldehyde and sinapaldehyde [1, 7, 16]. On the basis of kinetic studies where Kcat and Kcat/Km values for feruloyl CoA are highest in mixed substrate reaction having all the substrates in equal concentration, where coniferaldehyde is obtained as the major product along with a trivial amount of 5-hydroxyconiferaldehyde [1]. As calculated on the basis of Ki values in cocatalyzed reactions, feruloyl CoA is known to exert a strong competitive inhibition with other substrates of CCR, while the later exert a very weak inhibition with feruloyl CoA, revealing feruloyl as the most competitive inhibitor in CCR reaction [1, 7].

The present study addresses the homology model and docking analysis of CCR in the *Leucaena leucocephala*. The information from docking conformations will provide new insight to study the mechanism of CCR catalyzed enzymatic reactions. The approach is applicable in engineering 3D structures of enzymatic models, and studying interactions of active site residues with substrates [17].

Materials and methods

Sequence alignment and homology modeling of CCR

CCR protein sequence of *Leucaena leucocephala* (NCBI protein accession number: CAK22319) was selected. BLAST algorithm against Protein Data Bank (PDB) was used to carry out the sequence homology searches. The sequence and 3D structure of template proteins were extracted from the PDB database [18]. Multiple sequence alignments of the target and template sequences were carried out using ClustalW 2.0.10 program with default parameters [19]. High-resolution crystal structure of homologous protein as a template were considered for homology modeling. The coordinates of templates were used to build the initial models of CCR. The homology models of CCR were constructed using MODELLER 9v7 [20, 21]. The MODELLER generated models optimally satisfies spatial restrains, which includes homology-derived restraints on the distances and dihedral angles, stereo chemical restraints. Coordinates from the template proteins to the structurally conserved regions (SCRs), structurally variable regions (SVRs), N-termini and C-termini were assigned to the target sequence based on the satisfaction of spatial restraints. All side chains of the model protein were set by rotamers.

Energy minimization and simulations

The homology model obtained from the MODELLER was improved further by molecular dynamics and equilibration methods using Nano Molecular Dynamics (NAMD 2.5) [22] and Chemistry of Harvard Molecular Modelling (CHARMM27) force field for lipids and proteins [23, 24]. A 50,000-step minimization was employed in the simulation to remove all bad contacts of side chains. Minimum switching distance of 8.0 Å and a cut off of 12.0 Å for Vander Walls interactions was used. The pair list of the non-bonded interactions was recalculated every 20 steps with a pair list distance of 13.5 Å. All hydrogen atoms were included during the calculation.

```
2C29:     ------------MGSQS-ETVCVTGASGFIGSWLVMRLLERGYTVRATV
CCR :     MPAAAPAPTAANTTSSGSGQTVCVTGAGGFIASWIVKLLLERGYTVRGTV
                      .* * :********.***.**:*  **********.**

2C29:     RDPTNVKKVKHLLDLPKAETHLTLWKADLADEGSFDEAIKGCTGVFHVAT
CCR :     RNPDDSKNS-HLKELEGAEERLTLHKVDLLDLESVKAVINGCDGIIHTAS
          *:* : *:  ** :*  ** :*** *.** *  *.. .*:** *::*.*:

2C29:     PMDFESKDPENEVIKPTIEGMLGIMKSCAAAKTVRRLVFTSSAGTVNIQE
CCR :     PV---TDNPE-EMVEPAVNGAKNVIIAAAEAK-VRRVVFTSSIGAVYMDP
          *:   ::.:** *:::*:::*  .:: :.* ** ***:***** *:* ::

2C29:     HQLP--VYDESCWSDMEFCRAKKMTAWMYFVSKTLAEQAAWKYAKENNID
CCR :     SRNIDEVVDESCWSNLEYCKNTKN---WYCYGKAVAEQAAWDEAKARGVD
           :    * ******::*:*: .*     *  .*::******. ** ..:*

2C29:     FITIIPTLVVGPFIMSSMPPSLITALSPITGNEAHYSIIRQGQFVHLDDL
CCR :     LVVVNPVLVLGPLLQSTMNASTIHILKYLTGSAKTYANATQA-YVHVKDV
          ::.: *.**:**:: *:* .* *  *. :**.   *:   *. :**:.*:

2C29:     CNAHIYLFENPKAEGRYICSSHDCIILDLAKMLREKYPEYNIPTEFKG-V
CCR :     ALAHVLVYEIPSASGRYLCSESSLHRGELVEILAKYFPEYPIPTKCSDEK
          . **: ::* *.*.***:**. .    :*.::* : :*** ***: ..

2C29:     DENLKSVCFSSKKLTDLGFEFKYSLEDMFTGAVDTCRAKGLLPPSHEKPV
CCR :     NPRAKAYTFSNKRLKDLGLEFTPVHQCLYD-TVKSLQDKGHLPLPT----
          : . *:  **.*:*.***:**.   : ::  :*.: : ** ** .

2C29:     DGKT
CCR :     ----
```

Fig. 1 Sequence alignment of CCR with template. The asterisk indicates an identical or conserved residue; a colon indicates a conserved substitution; a dot indicates a semi-conserved substitution

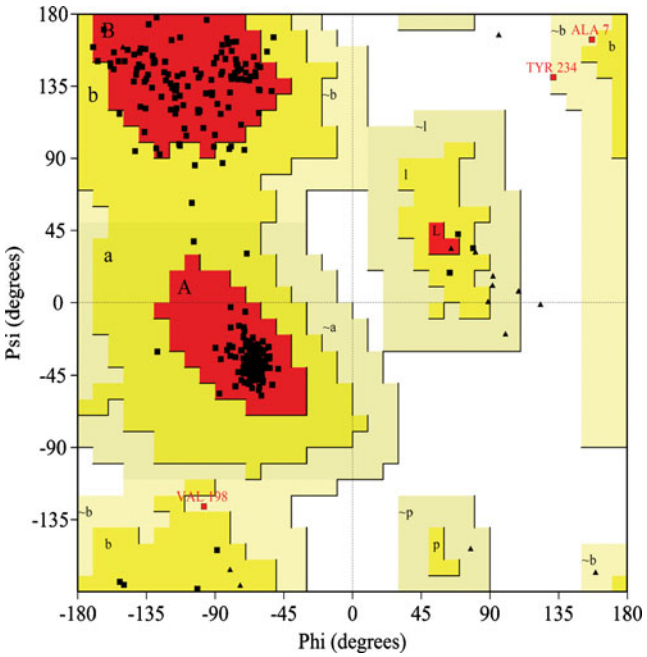

Fig. 2 Residue profile of CCR in Ramachandran's plot

Validation of predicted homology model

Structural and packing architecture of the modeled protein were calculated, *i.e.*, by calculating mean hydrogen bonds distances, mean dihedral angles, accessible surface area and packing volume, by using VADAR 1.4 program [25]. PROCHECK analysis [26] of the model was done to check that the residues were falling in the most favored region in the Ramachandran's plot. The resultant energy minimized protein models were used for the active site identification and for the docking analysis with substrate.

Active site identification

The substrate accessible pockets and active sites of CCR were identified by computed atlas of surface topography of proteins (CASTp) calculation [27] and CCDC GOLD [28–30]. The identified active sites were analyzed for amino acid cluster groups based on the solvent exposed active site atoms and bonding capacity of the polar groups. The substrate molecule feruloyl CoA, caffeoyl CoA, 5-hydroxyferuloyl CoA and sinapoyl CoA were downloaded from Pubchem database of NCBI [31], and converted to 3D structure with VEGA ZZ software [32].

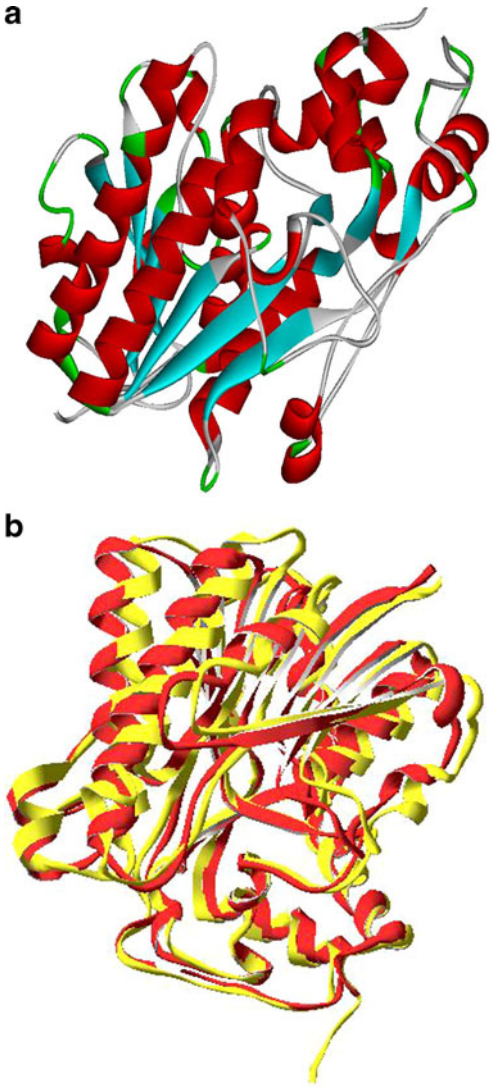

Fig. 3 (**a**) Homology model of Cinnamoyl CoA reductase (CCR) represented in ribbon diagram, (**b**) Superimposition of CCR and 3D structure of Dihydroflavonol-4-reductase (PDB entry 2C29.pdb), CCR represented in yellow and Dihydroflavonol-4-reductase represented in red color

Docking studies

Substrate molecules were docked to the binding sites by CCDC's GOLD (genetic optimization for ligand docking) [28–30]. One-hundred genetic algorithm (GA) runs were performed for each compound, and 10 ligand bumps were allowed in an attempt to account for mutual ligand/target

Table 2 Structural characteristics and features of the models

Protein	MHBD(Å)	MHBE	MHPh	MHPs	MCG^+	MCG^-	MRV ($Å^3$)	TV ($Å^3$)
CCR	2.2	−1.6	−64.9	−39.4	−66.5	62.5	139.8	46835.0

MHBD - Mean hydrogen bond distance; **MHBE** - Mean hydrogen bond energy; **MHPh -** Mean Helix Phi; **MHPs** - Mean Helix Psi; **MCG^+** – Mean Chi Gauche+; **MCG^-** - Mean Chi Gauche-; **MRV** - Mean residue volume; **TV** - Total volume (packing).

fit. The binding region for the docking study was defined as a 10 Å radius sphere centered on the active site. For each of the GA run a maximum number of 100,000 operations were performed on a population of 100 individuals with a selection pressure of 1.1. The number of islands was set to 5 with a niche size of 2. The weights of crossover, mutation, and migration were set to 95, 95, and 10 respectively. The scoring function Gold Score implemented in GOLD was used to rank the docking positions of the molecules, which were clustered together when differing by more than 2 Å rmsd. The best ranking clusters for each of the molecules were selected. Hydrogen bonds, bond lengths and close contacts between enzyme active site and substrate atoms were analyzed.

Results and discussion

Construction of model

Potential templates of target proteins, were obtained from the BLAST search for CCR. Template selection was performed on the basis of sequence similarity, residues completeness, crystal resolution and functional similarity. Table 1 shows the basic information on the selected template used in the study. Among the available candidate templates the sequence identities between target and templates are about ≤43%. In general, sequence identities of 30% are enough to construct the 3D model of target proteins through the homology modeling. 2C29.pdb was chosen as the template for the modeling of CCR. Its structure was solved as a ternary complex obtained with the oxidized form of nicotinamide adenine dinucleotide phosphate and dihydroquercetin. The model with the lowest value of the MODELLER objective function was selected as the best model for CCR. The final alignment of CCR and template (PDB ID: 2C29.pdb) with conservation was showed in Fig. 1.

Structural analysis of predicted models

Assessment of stereochemical properties of main-chain and side-chain residues was performed using Ramachandran plot. Figure 2 shows 91.9% of CCR residues are located in

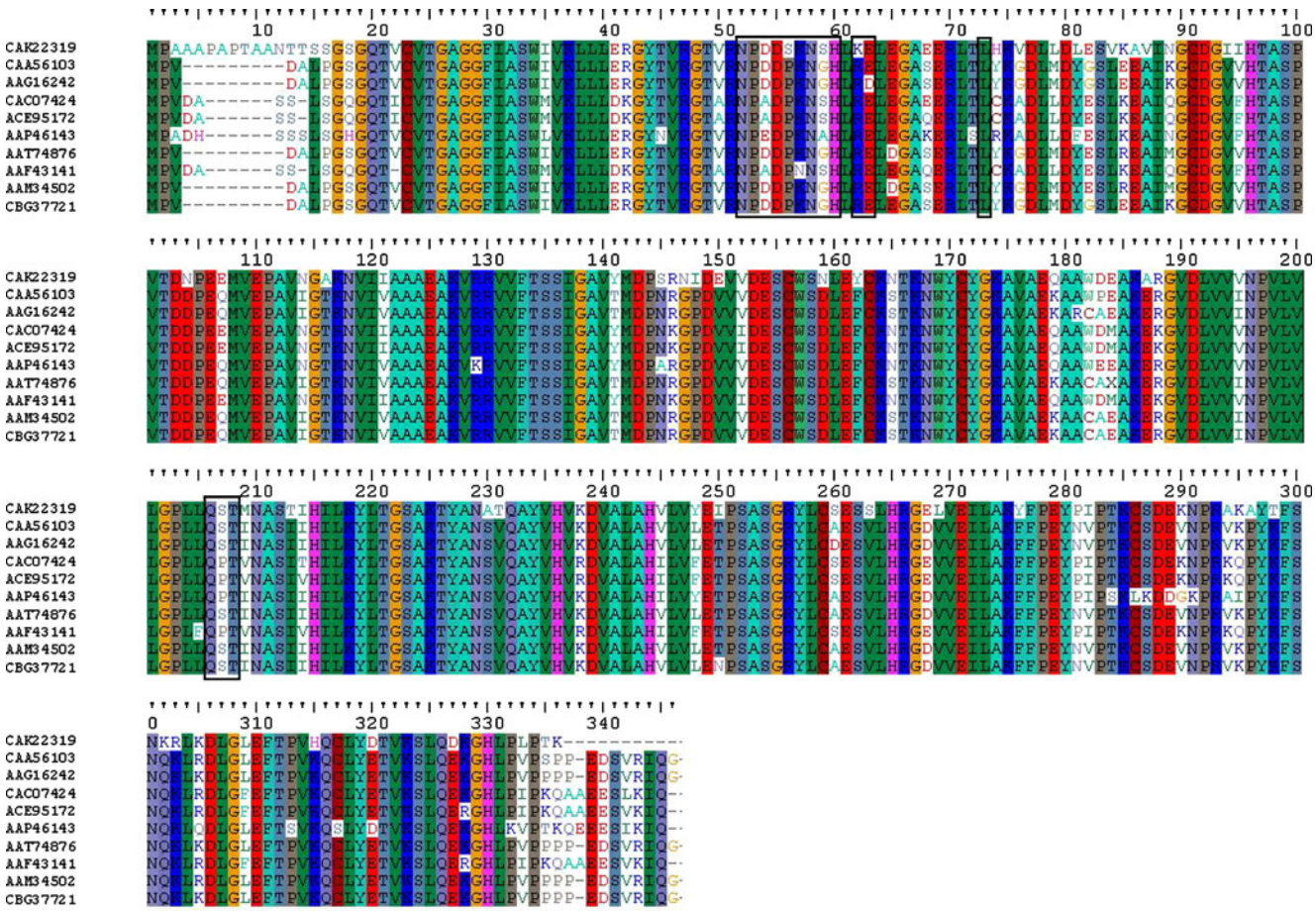

Fig. 4 Multiple sequence alignments of CCR homologues showing conserved regions and active site residues are marked in boxes

the most favoured regions, 7.1% residues in additional allowed regions and 1% residues in generously allowed regions in the Ramachandran plot of the selected model. The model which has above 90% of the residues falling in the most favorable region of Ramachandran plot was considered as a good model. In addition to mean helix phy, psi parameters and mean Chi Gauche values, the mean hydrogen bond distances and energy in the models were similar to the known protein crystal structures data. Mean residue volume in the model is 139.8 $Å^3$ and total packing volume of the model is 46835.0 $Å^3$, which shows very good packing architecture. All the structural parameters are shown in Table 2. The final model structure of CCR and superimposition of CCR and template were displayed in Fig. 3a and b. The central core region of this model mainly consists of β sheets surrounded by helices.

Catalytic active site prediction and docking studies

The sequences of CCR were observed conserved across number of plant species, in Fig. 4 multiple sequence alignments of CCR were presented. Figure 5 shows the predicted solvent exposed active site residues of the CCR. The solvent exposed active site residues are shaded in red color in spacefill model. Substrate binding site pocket is made up from 15 residues, *i.e.*, residues 52–60, 62–63, 73, and 206–208. Among these, seven residues are polar uncharged, six residues are polar charged and two residues are nonpolar hydrophobic. The active site residue conservation was marked in multiple alignments by boxes (Fig. 4). The residues 52, 53, 55, 58, 60, 73, 206, and

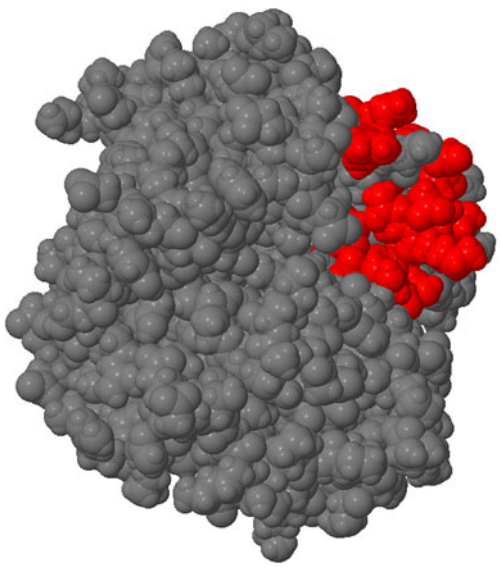

Fig. 5 Solvent exposed active site residues (red) of CCR, in space-fill representation

Table 3 Hydrogen bonding profile of docking conformations of CCR-feroloyl CoA

Docking Conformation No	Residues forming hydrogen bonds															Total H bonds
	GLY26	ALA27	GLY28	GLY29	THR49	ARG51	ASN52	ASP54	ASP55	SER56	LYS57	ASN58	LEU78	SER99	GLU107	GLN206	SER207	THR208	
1						4 Hb	1 Hb	1 Hb				2 Hb							8 Hb
2						1 Hb	2 Hb					3 Hb					1 Hb		7 Hb
3				1 Hb						1 Hb			1 Hb		1 Hb				4 Hb
4					1 Hb	1 Hb	2 Hb					3 Hb							7 Hb
5		1 Hb			1 Hb	4 Hb						1 Hb							7 Hb
6		1 Hb	1 Hb	2 Hb	2 Hb	1 Hb						1 Hb		1 Hb		1 Hb			10 Hb
7							1 Hb			1 Hb	2 Hb	1 Hb							5 Hb
8			1 Hb	1 Hb	3 Hb	2 Hb						2 Hb					1 Hb		10 Hb
9									1 Hb	2 Hb	1 Hb						1 Hb	1 Hb	6 Hb
10						4 Hb	2 Hb			3 Hb	1 Hb	1 Hb							11 Hb

Hb - Hydrogen bond

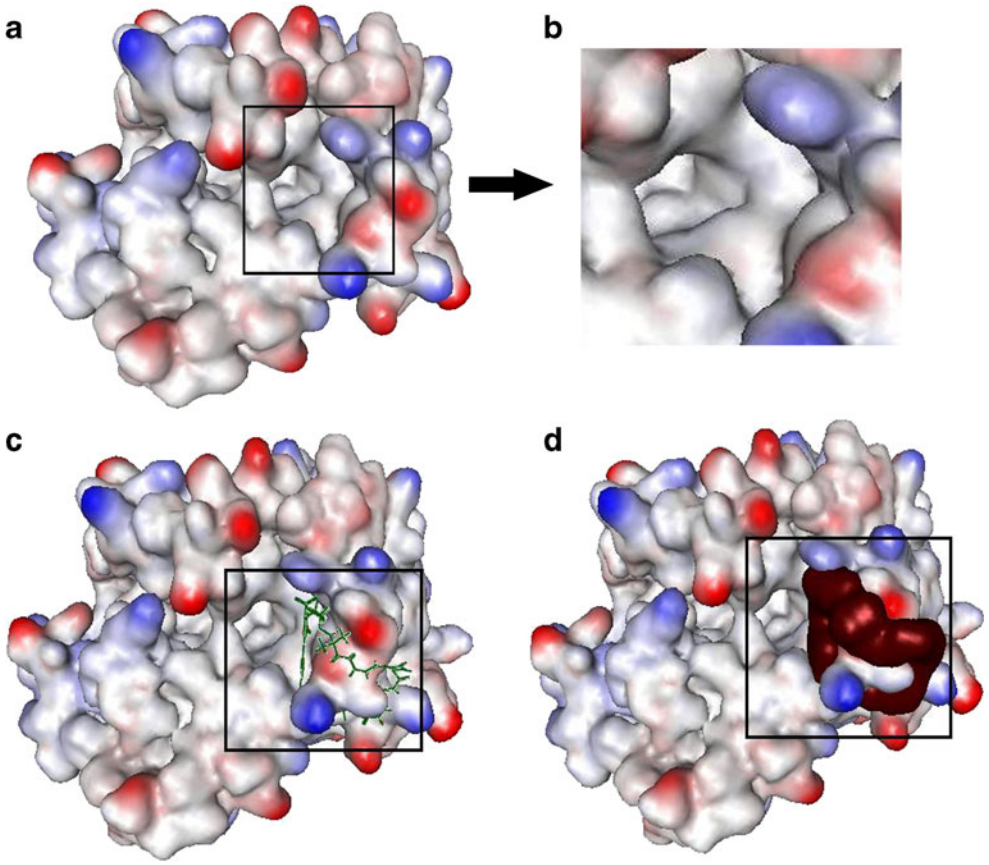

Fig. 6 Surface representation of catalytic active site in the CCR model (**a**) and close up view (**b**). Feruloyl CoA Conformation in the active site of CCR represented in both stick (**c**) and solid surface diagram (**d**)

208 are conserved in plant CCR sequences; in remaining active site residues 54 and 59 are variable. NADPH binding site pocket composed with residues ASP77, LEU78, LEU79, SER136, TYR180, PRO197, VAL198, LEU199 and SER212. In the template, active site for substrate binding comprises SER14, GLY15, PHE16, ILE17, VAL36, ARG37, LYS44, ASP64, LEU65, VAL84, ALA85, THR86, MET88, THR126, SER127, THR163, LYS167, PRO190, THR191, VAL193, PRO204, and SER205. However in case of CCR the substrate binding site residues are different, this is because of a different substrate. Perhaps the NADPH binding residues SER136, TYR180, PRO197, LEU199 and SER212 of CCR are conserved. Enzyme active site-feruloyl CoA docking was performed in 100 genetic algorithm runs which resulted in 10 highest score enzyme-substrate conformations. Among these, the best enzyme-substrate conformation was selected. The best enzyme-substrate interacting complex gives Gold fitness function score of 88.3428. Further, eight hydrogen bonds, involving residues ARG51, ASN52, ASP54 and ASN58, were observed to interact with the substrate atoms. Residue ARG51 forms four hydrogen bonds with substrate atoms, which is assumed as most active residue in the catalytic active site of CCR followed by ASN58 with only two hydrogen bonds. Table 3 describes the hydrogen bonding profile of docking conformations of CCR-feroloyl CoA. Figure 6 shows the active site cavity and

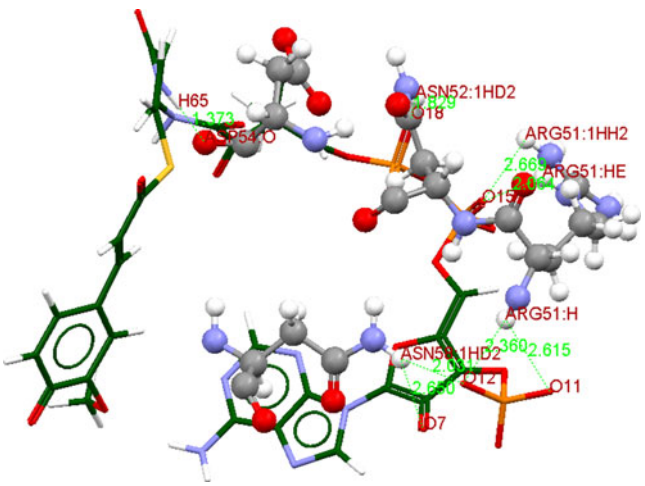

Fig. 7 Interaction of feruloyl CoA (stick form) with CCR catalytic active site residues ARG51, ASN52, ASP54, ASN58 (ball and stick form)

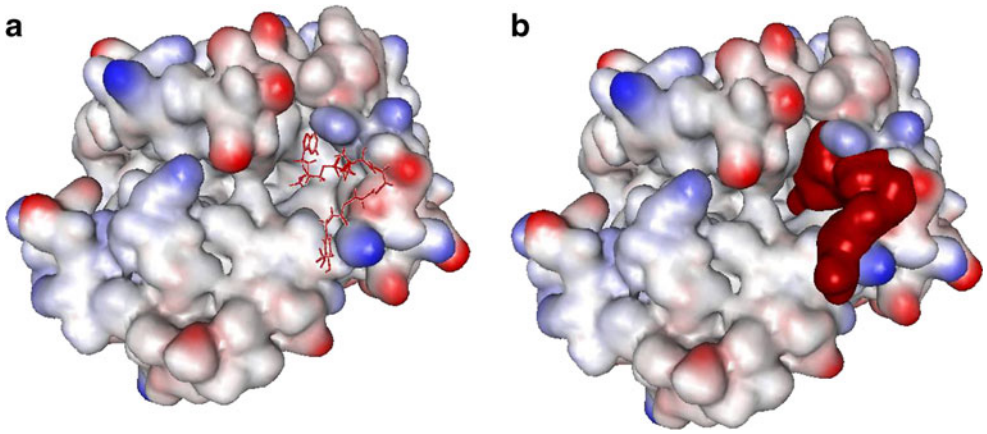

Fig. 8 5-hydroxyferuloyl CoA Conformation in the active site of CCR represented in both stick (**a**) and solid surface diagram (**b**)

feruloyl CoA binding conformation at active site. Figure 7 shows the hydrogen bond interactions between CCR and feruloyl CoA. All the hydrogen bond distances were observed within the range of 1.373 Å to 2.669 Å. The docking of CCR-feruloyl CoA interactions reveals that the residues ARG51, ASN52, ASP54 and ASN58 are involved in substrate binding. Interestingly, residue ARG51 is present just out side of the active site mouth pocket, enabling CCR-feluloyl CoA interaction more strong among the other substrates. Therefore in addition to the high number of hydrogen bond interactions, it is supposed to be most active residue in interacting complex.

Comparative analysis of CCR-substrates conformations

Docking conformations of all the substrates with CCR reveals that, CCR exhibits the highest Gold fitness function score of 88.3428 with feruloyl CoA. CCR Docking conformation with 5-hydroxyferuloyl CoA, caffeoyl CoA and sinapoyl CoA were shown with gold score of 57.0898, 46.6212 and 40.1429 respectively. 5-hydroxyferuloyl CoA forming 8 hydrogen bonds with residue GLY29, ALA32, ARG51, ASN52, ASN58, SER99 and SER207. The hydrogen bonds are in the range between 1.700 Å to 2.471 Å. The interacting residues are distantly placed in the sequence but due to usual protein folding they are closer. These residues are present at the active site cavity and produce productive binding with 5-hydroxyferuloyl CoA. The CCR-5-hydroxyferuloyl CoA docking conformation is shown in Fig. 8. Residues GLY28, ARG51, ASN52, ASP55 and ASN58 interact with Caffeoyl CoA by forming seven hydrogen bonds. Residue ARG51 forms three hydrogen bonds with caffeoyl CoA, and each of the remaining interacting residues GLY28, ASN52, ASP55 and ASN58 form only one hydrogen bond. The CCR-caffeoyl CoA conformation showing that the substrate is not fully accessing all the active site residues. The hydrogen bonds are in the range between 1.379 Å to 2.706 Å. The CCR- caffeoyl CoA docking conformation is presented in Fig. 9. Sinnapoyl CoA binds to residues ASP55, SER56, LYS57 and SER207 with seven hydrogen bonds. Residue LYS57 alone makes three hydrogen bonds, SER56 makes two hydrogen bonds and the remaining residues ASP55 and SER207 make one hydrogen bond

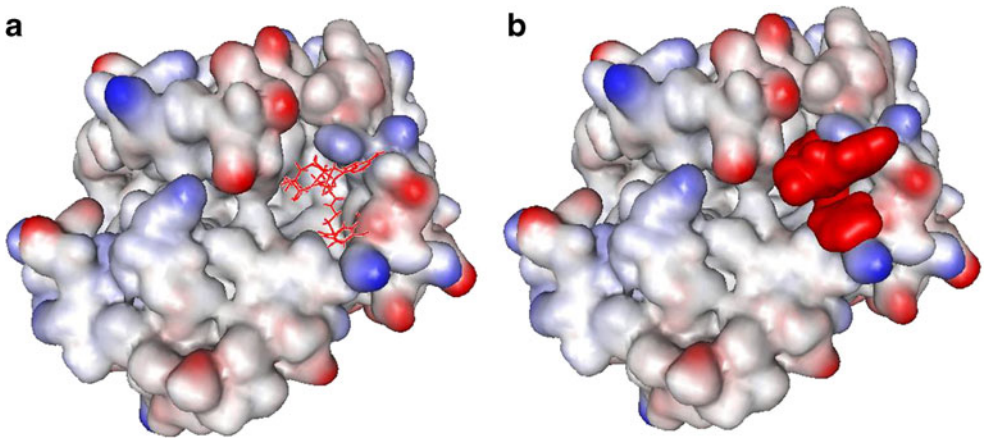

Fig. 9 Caffeoyl CoA Conformation in the active site of CCR represented in both stick (**a**) and solid surface diagram (**b**)

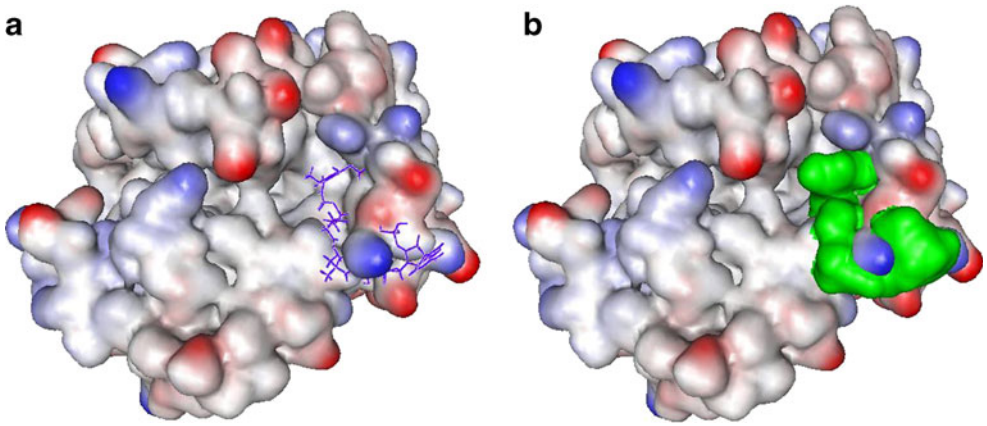

Fig. 10 Sinnapoyl CoA Conformation in the active site of CCR represented in both stick (**a**) and solid surface diagram (**b**)

each. The hydrogen bonds are in the range between 1.369 Å to 2.612 Å. The CCR- sinnapoyl CoA docking conformation is presented Fig. 10. The hydrogen bond interactions and gold scores of docking conformations are depicted in Table 4. The substrate binding residue profile shows that, only feruloyl CoA is interacting with charged polar aminoacids, where as other substrates are interacting with polar-uncharged and non-polar amino acids, due to this reason the CCR-feruloyl CoA interaction is stronger than other substrates.

Conclusions

CCR plays a prime role in the lignin biosynthesis pathway as it provides cinnamaldehyde intermediates for the formation of guaiacyl lignin and syringyl lignin. Homology model of CCR of *Leucaena leucocephala* showed 91.9% of residues fall in the most favorable region and 7.1% of residues are in the allowed region of Ramchandran plot, suggesting the modeled CCR structure was reliable for the docking studies. Top ten ranked CCR-feruloyl CoA docking conformation analysis reveals that, the feruloyl CoA binds at the mouth of the active site pocket. The best docking conformation showed residues ARG51, ASN52, ASP54 and ASN58 are involved in feruloyl CoA binding with eight hydrogen bonds. The residue ARG51 is present just outside the active site mouth and sharing half of the total hydrogen bonds with feruloyl CoA, this result concludes the active participation of ARG51 in the enzyme-substrate interaction. CCR-feruloyl CoA conformations showed, feruloyl CoA binds at the gateway to the active site. These docking studies deduce that the CCR-feruloyl CoA complex is stable to produce its product coniferaldehyde and will be involved in competitive inhibition of other substrates.

Table 4 Docking statistics of CCR and substrates

Substrate	Protein residues involved in bonding	Substrate atoms involved in bonding	Hydrogen bond distance (Å)	Gold Score
Feruloyl CoA	ARG51:H	O11, O12	2.615	88.3428
	ARG51:HH2	O15	2.360	
	ARG51:HE	O15	2.669	
	ASN52:1HD2	O18	2.064	
	ASP54:O	H65	1.829	
	ASN58:1HD2	O12	1.373	
	ASN58:1HD2	O7	2.031	
			2.650	
Caeffoyl CoA	GLY28:H	O20	2.476	46.6212
	ARG51:1HH2	N26	2.706	
	ARG51:NH2	H81	1.829	
	ARG51:NE	H81	1.379	
	ASN52:1HD2	N27	1.804	
	ASP55:OD1	H102	2.103	
	ASN58:1HD2	O20	2.182	
1,5-Hydroxyferuoyl CoA	GLY29:H	O13	2.471	57.0898
	ALA32:H	O13	2.323	
	ARG51:H	O16	1.710	
	ASN52:H	O19	2.267	
	ASN52:1HD2	O14	1.770	
	ASN58:1HD2	O15	1.700	
	SER99:H	O7	2.113	
	SER207:HG	O23	2.119	
Sinnapoyl CoA	ASP55:OD1	H82	1.369	40.1429
	SER56:OG	H70	1.942	
	SER56:H	O12	1.811	
	LYS57:H	O12	2.612	
	LYS57:HZ1	O6	2.549	
	LYS57:HZ1	O11	1.793	
	SER207:HG	O18	1.749	

Acknowledgments Research in VV's laboratory is supported by XI OBC plan grant of University of Hyderabad. The authors wish to thank Prof. U.M.X. Sangodkar for his valuable suggestions.

References

1. Li L, Cheng X, Lu S, Nakatsubo T, Umezawa T, Chiang VL (2005) Clarification of cinnamoyl co-enzyme a reductase catalysis in monolignol biosynthesis of aspen. Plant Cell Physiol 46:1073–1082
2. Thumma BR, Nolan MF, Evans R, Moran GF (2005) Polymorphisms in Cinnamoyl CoA Reductase (CCR) are associated with variation in microfibril angle in eucalyptus spp. Genetics 171:1257–1265
3. Lacombe E, Hawkins S, Doorsselaere JV, Piquemal J, Goffner D et al. (1997) Cinnamoyl CoA reductase, the first committed enzyme of the lignin branch biosynthetic pathway: Cloning, expression and phylogenetic relationships. Plant J 11:429–441
4. Lauvergeat V, Rech P, Jauneau A, Guez C, Coutos-Thevenot P et al. (2002) The vascular expression pattern directed by the Eucalyptus gunnii cinnamyl alcohol dehydrogenase Eg CAD2 promoter is conserved among woody and herbaceous plant species. Plant Mol Biol 50:497–509
5. Baltas M, Lapeyre C, Bedos-Belval F, Maturano M, Saint-Aguet P, Roussel L, Duran H, Grima-Pettenati J (2005) Kinetic and inhibition studies of cinnamoyl-CoA reductase 1 from Arabidopsis thaliana. Plant Physiol Biochem 43:746–753
6. Dixon RA, Chen F, Guo D, Parvathi K (2001) The biosynthesis of monolignols: a 'metabolic grid', or independent pathways to guaiacyl and syringyl units. Phytochemistry 57:1069–1084
7. Kawasaki T, Koita H, Nakatsubo T, Hasegawa K, Akabayashi K, Akahashi H, Umemura K, Umezawa T, Shimamoto K (2006) Cinnamoyl-CoA reductase, a key enzyme in lignin biosynthesis, is an effector of small GTPase Rac in defense signaling in rice. PNAS 103:230–235
8. Ma QH (2007) Characterization of a cinnamoyl-CoA reductase that is associated with stem development in wheat. J Exp Bot 58:2011–2021
9. Moershbacher B, Noll U, Gorrichon L, Reisener HJ (1990) Specific inhibition of lignifications breaks hypersensitive resistance of wheat to stem rust. Plant Physiol 93:465–470
10. Boerjan W, Ralph J, Baucher M (2003) Lignin biosynthesis. Annu Rev Plant Biol 54:519–546
11. Jones L, Ennos AR, Turner SR (2001) Cloning and characterization of irregular xylem4 (irx4): a severely lignin-deficient mutant of Arabidopsis. Plant J 26:205–216
12. Luderitz T, Grisebach H (1981) Enzymic synthesis of lignin precursors. Comparison of cinnamoyl-CoA reductase and cinnamyl alcohol: NADP+ dehydrogenase from spruce (Picea abies L.) and soyabean (Glycine max L.). Eur J Biochem 119:115–124
13. Goffner D, Cambell MM, Campargue C, Clastre M, Borderies G, Boudet A, Boudet AM (1994) Purification and characterization of cinnamoyl-coenzyme A: NADP oxidoreductase in Eucalyptus gunii. Plant Physiol 106:625–632
14. Piquemal J, Lapierre C, Myton K, O' Connel A, Schuch W, Grima-Pettenati J, Boudet AM (1998) Down-regulation of cinnamoyl- CoA reductase induces significant changes of lignin profiles in transgenic tobacco plants. Plant J 13:71–83
15. Sarni F, Grand C, Boudet AM (1984) Purification and properties of cinnamoyl-CoA reductase and cinnamyl alcohol dehydrogenase from poplar stems (Populus X euramerican). Eur J Biochem 139:259–265
16. Meng H, Campbell WH (1998) Substrate profiles and expression of caffeoyl coenzyme A and caffeic acid O-methyltransferases in secondary xylem of aspen during seasonal development. Plant Mol Biol 38:513–520
17. N Phogat, V Vindal, V Kumar, Krishna K Inampudi, Nirmal K Prasad (2010) Sequence analysis, in silico modeling and docking studies ofCaffeoyl CoA-O-methyltransferase of Populus trichopora. J Mol Model (In Press)
18. Berman HM, Westbrook J, Feng Z, Gilliland G, Bhat TN, Weissig H, Shindyalov IN, Bourne PE (2000) The protein data bank. Nucleic Acids Res 28:235–242
19. Larkin MA, Blackshields G, Brown NP, Chenna R, McGettigan PA, McWilliam H, Valentin F, Wallace IM, Wilm A, Lopez R, Thompson JD, Gibson TJ, Higgins DG (2007) Clustal W and clustal X version 2.0. Bioinformatics 23:2947–2948
20. Sali A, Blundell TL (1993) Comparative protein modelling by satisfaction of spatial restraints. J Mol Biol 234:779–815
21. Eswar N, Marti-Renom MA, Webb B, Madhusudhan MS, Eramian D, Shen M, Pieper U, Sali A (2006) Comparative protein structure modeling with MODELLER. Current protocols in bioinformatics. Wiley, Suppl 15, 5.6.1-5.6.30
22. Phillips JC, Braun R, Wang W, Gumbart J, Tajkhorshid E, Villa E, Chipot C, Skeel RD, Kale L, Schulten K (2005) Scalable molecular dynamics with NAMD. J Comput Chem 26:1781–1802
23. MacKerell AD Jr, Brooks B, Brooks CL III, Nilsson L, Roux B, Won Y, Karplus M (1998) CHARMM: The energy function and its parameterization with an overview of the program. In: Schleyer PVR et al. (eds) The encyclopedia of computational chemistry 1. Wiley, Chichester, pp 271–277
24. MacKerell AD et al. (1998) All-atom empirical potential for molecular modeling and dynamics studies of proteins. J Phys Chem B 102:3586–3616
25. Willard L, Ranjan A, Zhang H, Monzavi H, Boyko RF, Sykes BD, Wishart DS (2003) VADAR: a web server for quantitative evaluation of protein structure quality. Nucleic Acids Res 31:3316–3319
26. Laskowski RA, MacArthur MW, Moss DS, Thornton JM (1993) PROCHECK: a program to check the stereochemical quality of protein structures. J Appl Crystallogr 26:283–291
27. Dundas J, Ouyang Z, Tseng J, Binkowski A, Turpaz Y, Liang J (2006) CASTp: computed atlas of surface topography of proteins with structural and topographical mapping of functionally annotated residues. Nucleic Acids Res 34:W116–118
28. Jones G, Willett P, Glen RC (1995) Molecular recognition of receptor sites using a genetic algorithm with a description of desolvation. J Mol Biol 245:43–53
29. Jones G, Willett P, Glen RC, Leach AR, Taylor R (1997) Development and validation of a genetic algorithm for flexible docking. J Mol Biol 267:727–748
30. Verdonk ML, Cole JC, Hartshorn MJC, Murray W, Taylor RD (2003) Improved protein-ligand docking using GOLD. Proteins 52:609–623
31. Wang Y, Xiao J, Suzek TO, Zhang J, Wang J, Bryant SH (2009) PubChem: a public information system for analyzing bioactivities of small molecules. Nucleic Acids Res 6:1–11
32. Pedretti A, Villa L, Vistoli G (2004) VEGA - An open platform to develop chemo-bioinformatics applications, using plug-in architecture and script" programming". J Comput Aided Mater Des 18:167–173